International Journal of Nanomedicine

Dovepress
open access to scientific and medical research

Open Access Full Text Article

ORIGINAL RESEARCH

Copper-Based Single-Atom Nanozyme System Mimicking Platelet Cells for Enhancing the Outcome of Radioimmunotherapy

Cheng Chen[1,*], Nandi Chen[2,3,*], Yan Qi[1,*], Meng Lyu[2], Chaoyan Wu[4,*], Conghua Xie[1], Haijun Yu[1]

[1]Department of Radiation and Medical Oncology, Hubei Province Cancer Clinical Study Center, Hubei Key Laboratory of Tumor Biological Behaviors, Zhongnan Hospital of Wuhan University, Wuhan, Hubei, 430071, People's Republic of China; [2]Department of Gastrointestinal Surgery & Department of Geriatrics, Shenzhen People's Hospital (The Second Clinical Medical College, Jinan University, The First Affiliated Hospital, Southern University of Science and Technology), Shenzhen, Guangdong, 518020, People's Republic of China; [3]Analysis and Testing Center, Shenzhen Technology University, Shenzhen, 518118, People's Republic of China; [4]Department of Integrated Traditional Chinese Medicine and Western Medicine, Zhongnan Hospital of Wuhan University, Wuhan, Hubei, 430071, People's Republic of China

*These authors contributed equally to this work

Correspondence: Haijun Yu; Conghua Xie, Email haijunyu@whu.edu.cn; chxie_65@whu.edu.cn

Background: Radiotherapy is an indispensable part of the multidisciplinary treatment of breast cancer (BC). Due to the potential for serious side effects from ionizing radiation in the treatment of breast cancer, which can adversely affect the patient's quality of life, the radiation dose is often limited. This limitation can result in an incomplete eradication of tumors.

Methods: In this study, biomimetic copper single-atom catalysts (platelet cell membrane camouflaging, PC) were synthesized with the aim of improving the therapeutic outcomes of radiotherapy for BC. Following guidance to the tumor site facilitated by the platelet cell membrane coating, PC releases a copper single-atom nanozyme (SAzyme). This SAzyme enhances therapeutic effects by generating reactive oxygen species from H_2O_2 and concurrently inhibiting the self-repair mechanisms of cancer cells through the consumption of intracellular glutathione (GSH) within the tumor microenvironment. PC-augmented radiotherapy induces immunogenic cell death, which triggers an immune response to eradicate tumors.

Results: With the excellent biocompatibility, PC exhibited precise tumor-targeting capabilities. Furthermore, when employed in conjunction with radiotherapy, PC showed impressive tumor elimination results through immunological activation. Remarkably, the tumor suppression rate achieved with PC-enhanced radiotherapy reached an impressive 93.6%.

Conclusion: Therefore, PC presents an innovative approach for designing radiosensitizers with tumor-specific targeting capabilities, aiming to enhance the therapeutic impact of radiotherapy on BC.

Keywords: platelet cell membrane, single-atom nanozyme, radiotherapy, radioimmunotherapy, breast cancer

Introduction

Breast cancer (BC) stands as one of the most frequently diagnosed cancers among females globally.[1] In clinical practice, a combination of surgery, chemotherapy, and radiotherapy is often recommended as adjuvant treatments to achieve more favorable therapeutic outcomes.[2] In particular, post breast-conserving surgery, radiotherapy significantly reduces the rate of tumor recurrence by nearly half.[3,4] Nevertheless, the planning of radiotherapy for breast cancer presents a challenge, as it requires meticulous care to prevent radiation-induced damage to nearby healthy tissues and surrounding organs at risk (OAR).[5,6] Hence, the radiotherapy mice cause severe side effects or raise the risk of secondary cancers due to incomplete elimination of tumors. Another issue linked to recurrence following radiotherapy for breast cancer is the radio-resistance exhibited by tumor cells.[6,7] This resistance is attributed to the complex tumor microenvironment, characterized by conditions such as hypoxia and the overexpression of (GSH) and H_2O_2.[8–10] Therefore, in order to attain the desired level

Received: 20 October 2023
Accepted: 13 December 2023
Published: 15 January 2024

of tumor control while also safeguarding normal tissues and organs, it becomes imperative to harness nanotechnology for the effective enhancement of radiotherapy in the treatment of breast cancer.[11,12]

Nanozymes, a category of nanostructured materials exhibiting catalytic properties akin to natural enzymes, have garnered considerable interest in various fields such as biosensing, environmental applications, and tumor therapy in recent times.[13–15] In contrast to their natural counterparts, nanozymes offer several advantages, including exceptional stability, cost-effectiveness, and resilience in relatively harsh conditions, making them highly promising for a range of applications.[16] Previously, Yan reported on the use of nanoparticles (NPs) of iron oxide with peroxidase-like (POD-like) catalytic abilities, which has since spurred research and development efforts in the design and utilization of nanozymes.[17] Nanozymes exhibiting POD or oxidase (OD) activity plays a role in the regulation of reactive oxygen species (ROS), converting H_2O_2 to facilitate cell death.[18,19] Additionally, nanozymes mimicking catalase (CAT) and superoxide dismutase (SOD) functions can generate abundant oxygen to alleviate hypoxic conditions.[20,21] The tumor microenvironment often contains an abundance of GSH, which can impede the therapeutic effectiveness of chemotherapy drugs by aiding in the repair of damage within tumor cells. Hence, nanozymes that have the capability to deplete GSH, like Ang-IR780-MnO_2-PLGA, serve to modulate the intratumoral microenvironment, thereby mitigating the progression of the tumor.[22] In recent times, single-atom nanozymes (SAzymes) have gained prominence due to their precisely defined nanostructures, offering the highest atomic utilization efficiency.[15,23–25] Among these, manganese-based SAzymes exhibit POD-like and CAT-like properties. When subjected to laser irradiation, these SAzymes disrupt the redox balance, leading to cancer cell death through the Fenton reaction.[10] Single cobalt (Co) atoms, when loaded onto nitrogen-doped porous carbon centers, can serve as mimics for CAT and OD, generating $O_2^{\cdot -}$ radicals effectively and ultimately inducing cell death.[26] It is promising for multifunctional SAzymes to be introduced as adjuvants in various treatment approaches, aiming to achieve enhanced and efficient treatment outcomes.

Radiotherapy produces ROS through the process of water radiolysis, which is crucial for inducing cell death. However, the efficacy of radiation treatment is impeded by radio-resistance attributed to the unique tumor microenvironment characterized by hypoxia.[27] In addition, radiation dosage is often limited to prevent harm to OAR and minimize side effects. Hence, noble metals are being developed as radio-sensitizers to augment the production of ROS induced by radiotherapy.[27–31] Other strategies, such as oxygen delivery or oxygen generation, have been employed in the design of radio-sensitizers.[32,33] However, when utilized for treatment, nanozymes face challenges such as low immunogenicity and a lack of T cell infiltration within tumors, which hinder their efficacy in treating tumors.[34,35] Therefore, in order to amplify the overall treatment effectiveness, we have created a copper (Cu)-based single-atom nanozyme referred to as Cu SAZ, which incorporates platelet cell membrane camouflaging (PC) to enhance radiosensitization (Scheme 1). The application of platelet cell membrane coating serves to prolong blood circulation and prevent immune clearance of PC

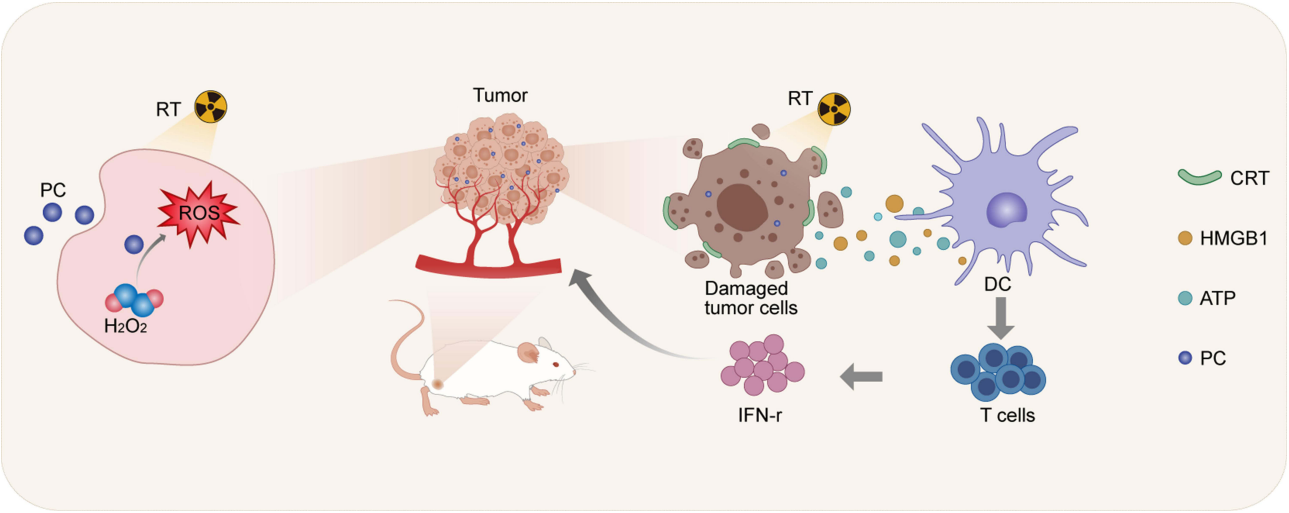

Scheme 1 Schematic illustration of PC-enhanced radioimmunotherapy.

through surface modifications, ultimately optimizing its therapeutic potential. By selecting copper to fabricate the nanozyme, within the slightly acidic tumor microenvironment, PC facilitates the intracellular decomposition of H_2O_2 decomposition into toxic ROS within tumor cells. This addresses the shortfall in ROS production that typically occurs during radiotherapy, ultimately resulting in the death of cancer cells. This approach, which effectively generates an ample amount of ROS, has been demonstrated to possess a remarkable capacity for inducing immunogenic cell death (ICD) within tumors. It activates a highly efficient immunotherapeutic response in a murine model. With its excellent biocompatibility, PC exhibits outstanding antitumor efficacy when combined with radiotherapy in both in vitro and in vivo experiments. These findings highlight its clinical potential for enhancing cancer radioimmunotherapy.

Experimental Section

Preparation and Characterization of the Biomimetic Single-Atom Nanozyme System (PC)

PC was prepared by a previously reported method.[23] Platelet cell membranes were derived by a repeated freeze–thaw process. Aliquots of platelet cell membrane suspensions were first frozen at −80 °C, thawed at room temperature, then centrifugated (4000 × g, 3 min). After purification with PBS mixed with protease inhibitor tablets, the pelleted platelet cell membranes were resuspended in water, sonicated in a capped glass vial and then extruded through 400 polycarbonate porous membranes and then a 200 nm polycarbonate on a mini extruder (AvantiPolar Lipids, USA). The cell membrane vesicles were hereby obtained. The platelet cell membrane vesicles derived from 20 μL of murine blood were first mixed with 100 μg/mL of Cu SAZs. Then, the solution was extruded through a polycarbonate porous membrane in a mini-extruder. The resultant production was then centrifugated for 10 min at 1000 × g to remove the remaining platelet cell membrane. Next, the production which is termed PC was collected and stored at 4 °C in PBS. A similar approach was used to synthesize a red blood cell membrane-coated single-atom nanozyme system (RC). RBC membranes were obtained via a previously reported low-osmosis method.[36] All subsequent steps were identical to those used to synthesize PC.

Detection of ROS Generation, DNA Damage and CRT Expression

We further investigate ROS production and DNA damage in various treatment groups (PBS; RT; PC; RC+RT; PC+RT). Cells were seeded in confocal culture dishes and cultured for 24 h. Subsequently, the medium was replaced by 2 mL RPMI-1640 containing 10% fetal bovine serum (FBS) containing PC (40 μg/mL) or RC (equivalent mole dosage of 40 μg/mL of PC) with 1 Mm GSH and 100 μM H_2O_2 for 4 h incubation. Then, cells were irradiated with 6 Gy radiotherapy or not. Then, cells were stained with DCFH-DA, γ-H_2AX-specific and anti-Calreticulin and observed by fluorescence microscopy.

Animals Model

Six-week old female balb/c mice were purchased from Beijing Vital River Company (Beijing, China). All the animals were fed in an animal facility under filtered air conditions (22–25°C) in cages with wood shavings for bedding. All animal experiments were conducted according to the guidelines for Care and Use Committee of Zhongnan Hospital of Wuhan University and approved by the Animal Care Committee of the Laboratory Animals at Zhongnan Hospital of Wuhan University (No. WP20230077). 100 μL PBS containing 10^6 4T1 cells were subcutaneously injected on the right lap to establish subcutaneous tumor model.

Fluorescence Imaging in vivo

When tumor volume reached about 200 mm^3, mice were divided randomly into 2 groups and received injection of DiO labeled RC or PC via tail vein. Then, the biodistribution of nanoparticles in mice was observed using a fluorescence imaging system at 6 h, 12 h and 24 h post injection.

Tumor Treatment Assessment

Mice with tumor volume at 200 mm^3 were divided into 5 groups and subjected to the following treatments: PBS (100 μL); RT (6 Gy); PC (5 mg/kg); RC (equivalent mole dosage of 40 μg/mL of PC) +RT; PC+RT. The day mice received

treatment was set as day 1. Then, the body weight and tumor volume of mice in each group were monitored every third day. Tumors were harvest for Ki67, TUNEL and HE staining. Tumors in each treatment groups were collected and cut into small pieces. Then, small pieces were digested and filtered to obtain cell pellet. Next, single-cell suspension was stained with CD8-Percp and CD4-BV610 and analyzed with flow cytometry.

For more experimental methods, please refer to Supplementary Methods.

Result and Discussion

The synthesis of PC NPs comprised three key steps. Initially, a Cu-based single-atom nanozyme (Cu SAZ) was prepared using a pyrolysis method.[23,37] As illustrated in Figure 1A, examination via transmission electron microscopy (TEM) confirmed that Cu SAZ exhibited a uniform spherical structure with an approximate diameter of 285 nm. We then used aberration-corrected high-angle annular dark-field scanning transmission electron microscopy (AC-HAADF-STEM) to validate the isolated bright dots, which confirmed the existence of single Cu atoms (Figure 1B). Next, the platelet cell membrane was extracted from cells by a repeated freeze–thaw process. Then, cell membrane vesicles and Cu SAZ NPs were extruded through a 200 nm membrane using a mini-extruder. Subsequently, the product underwent additional purification through centrifugation to eliminate any surplus cell membrane vesicles, resulting in the acquisition of PC NPs. The morphological structure of these PC NPs is illustrated in Figure 1C. An outer thin film had surrounded the Cu SAZ NPs, with a thickness of approximately 4 nm, closely resembling the thickness of a phospholipid bilayer membrane. Further element analysis of mapping and energy-dispersive X-ray spectroscopy (EDX) confirmed the presence of copper element in PC (Figures S1 and S2). The dynamic light scattering (DLS) results revealed that the size distribution of PC NPs was 290.5 nm (Figure 1D). The stability of PC NPs in PBS and a medium containing 10% FBS were evaluated. As shown in Figure 1E, PC NPs maintained a stable average hydrodynamic particle size in both mediums throughout the 7-day observation period. Subsequently, we evaluated the zeta potential of Cu SAZ, platelet membrane vehicles (PM), and PC. Following the camouflage of PM, which originally had a zeta potential of −16.8 eV, the zeta potential shifted from −11.4 eV to −15.3 eV, further confirming the successful coating of PC (Figure 1F). These results above indicate the successful fabrication of PC.

The red blood cell membrane can effectively camouflage nanoparticles, preventing their elimination by the immune system and thereby extending the circulation of nano-drugs in the bloodstream. Subsequently, we conducted a comparison to assess the targeting capability of red blood cell-camouflaged Cu SAZ (RC) in contrast to PC NPs. The red blood cell membrane was obtained using a cell lysis method. Subsequently, the red blood cell membrane-coated Cu SAZ was synthesized by extracting both the red blood cell membrane and Cu SAZ through a mini-extruder. The results of WB analysis of red blood cell membrane, platelet cell membrane, RC and PC in Figure S3 validated the comparable protein content of CD62-p (p-selectin) and CD41 between PC and the platelet cell membrane, affirming the successful coating of the platelet cell membrane onto PC. The Fourier-transform infrared spectroscopy (FTIR) spectrum in Figure S4 proved the existence of phospholipid protein in PC. Since large amount of disease-related binding markers were decorated on the surface of platelet cell membrane, PC was supposed to be efficient at targeting to tumor cells.[38] Therefore, 4T1 cells were co-incubated with DiO-labeled RC and PC NPs. After a 24-hour co-incubation period, the cell nuclei were stained with 4,6-Diamidino-2-phenylindole, dihydrochloride (DAPI, blue) and examined using confocal laser scanning microscopy (CLSM). As illustrated in Figure 1G, cells that were pre-treated with PC NPs exhibited a more pronounced red fluorescence when compared to the RC counterparts, which was due to the inherited physiological features including interaction with tumor cellsThis suggests that a larger quantity of NPs was internalized by the 4T1 cells.

On the basis of the characterization results provided above, the study proceeded to assess the impact of PC NPs in improving radiotherapy on 4T1 cells. Initially, the research focused on investigating the cytotoxic effects of PC and RC NPs on normal human breast epithelial cells (MCF-10A). The results indicated that the cell survival rate remained above 85% even at a Cu SAZ concentration of 50 μg/mL (Figure S5). This observation underscores the excellent biocompatibility of both PC and RC NPs, a crucial factor for their use as radiosensitizers. Encouraged by these findings, we subsequently delved into the examination of radiotherapy enhancement using PC. We employed 2′,7′-dichlorodihydrofluorescein diacetate (DCFH-DA), which transforms into 2′,7′-dichlorofluorescein (DCF) and emits green fluorescence in the presence of reactive oxygen species (ROS). Consequently, we utilized DCFH-DA as a probe to indicate the presence of ROS. As shown in Figure 2A, the RT and PC groups exhibited relatively low green

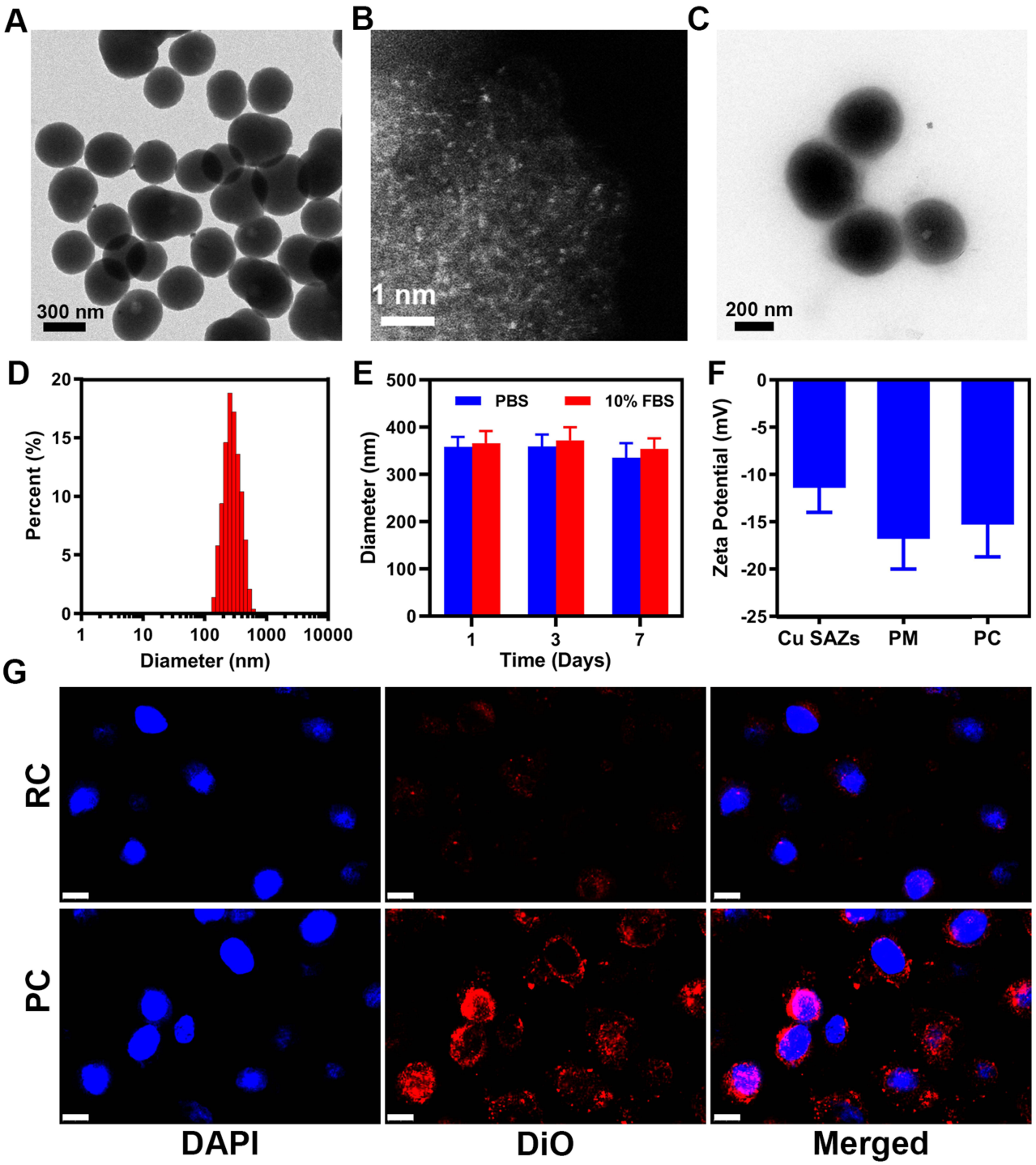

Figure 1 Characterization. (**A**) TEM images of Cu SAZs. (**B**) AC-STEM image of Cu SAZs, exhibiting Cu single atoms. (**C**) TEM images of PC. (**D**) Size-distribution profile of PC. (**E**) Diameter measurement of PC when dispersed in PBS and PBS with 10% FBS for 1, 3, and 7 days. (**F**) Zeta potential of Cu SAZs, PM, and PC. (**G**) Fluorescence images illustrating the cellular uptake of PM and PC (Scale bar: 10 μm).

fluorescence levels. In contrast, the vast majority of cells in the PC+RT group displayed robust green fluorescence, signifying a heightened production of ROS. It is worth noting that radiotherapy primarily induces cell death through the occurrence of DNA double-strand breaks. Hence, the extent of DNA damage in different treatment groups was assessed using γ-H_2AX immunofluorescence. In line with the findings from ROS staining, a prominent red fluorescence signal indicative of a high degree of DNA damage was evident in the PC+RT group. Subsequently, we examined cell viability

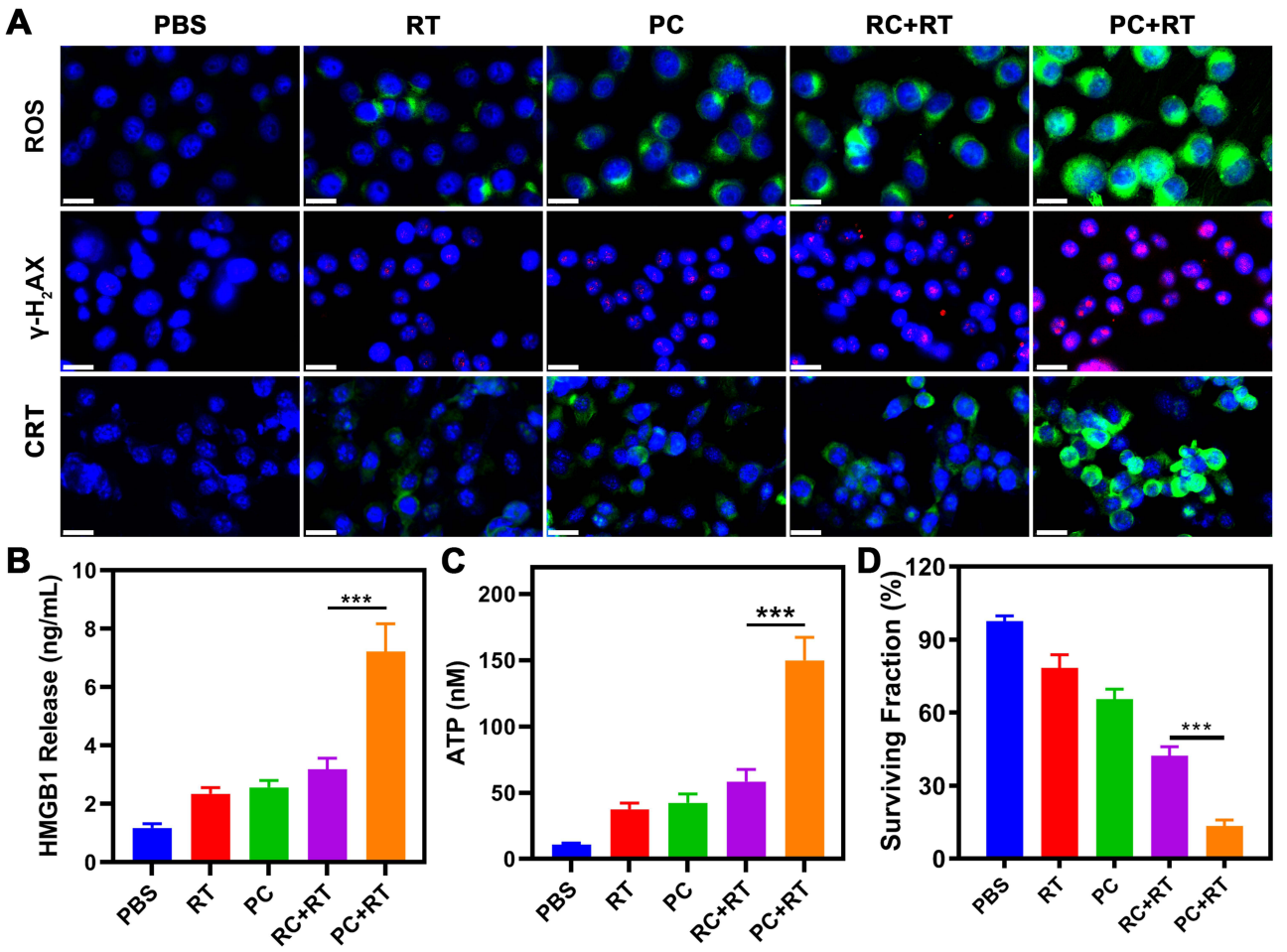

Figure 2 Radiosensitization and ICD induced by PC in the 4T1 tumor cell line. (**A**) ROS, γ-H_2AX, and CRT staining in various treatment groups (Scale bar: 20 μm). (**B**) HMGB1 release and (**C**) ATP content in the supernatant in various treatment groups. (**D**) Cell surviving fraction of 4T1 cells in different treatment groups. One-way ANOVA for multiple groups were applied for statistical analysis. ***$p < 0.001$.

using the CCK-8 kit in each experimental group. As shown in Figure S6, when compared to the group treated with RC +RT, which exhibited a cell viability of 61%, the cell viability significantly decreased to 41% in the PC+RT group. This suggests a more effective cell-killing effect with PC+RT.

To further investigate the activation of an immune response, we proceeded to evaluate molecules associated with immunogenic cell death (ICD). The treatment of PC+RT on 4T1 cells resulted in a substantial exposure of calreticulin (CRT) with notably higher green fluorescence intensity (Figure 2A). A mild release of high mobility group box-1 protein (HMGB1) and adenosine triphosphate (ATP) was detected in the RC, PC, and RC+RT groups (Figure 2B and C). In striking contrast, the secretion of HMGB1 and ATP was notably up-regulated in the PC+RT group. This heightened release of danger signals associated with ICD strongly implies that PC+RT can efficiently trigger the activation of the immune system, thereby further suppressing tumor cell proliferation. Moreover, colony formation assays were conducted to confirm the feasibility of PC+RT in inhibiting cell proliferation, as depicted in Figure 2D. These observed phenomena collectively validate the enhancement of the therapeutic effect of radiotherapy by PC in an in vitro setting.

Encouraged by the results regarding the cellular uptake by tumor cells, we proceeded to assess the biodistribution of PC and RC. Due to platelet-aggregating activity of tumor, nanoparticles with platelet cell membrane coating tend to allocate in tumor region.[36,37,39] For this purpose, mice with subcutaneous tumors on their right flank were intravenously injected with DiL-labeled PC and RC. An in vivo imaging system (IVIS) was employed to capture fluorescence images depicting the biodistribution of the NPs at various time intervals following injection. The

findings showed a more intense fluorescence signal in the tumors of mice treated with PC compared to those treated with RC at the 12-hour post-injection time point. This observation underscores the tumor-specific targeting capability of PC (Figure 3A). Biodistribution study proved that RC tends to accumulate in liver while PC allocated in tumor (Figure S7). Immunofluorescence staining of tumor sections in the two groups is presented in Figure 3B. A notably stronger red fluorescence intensity was detected in the PC group, indicating that PC exhibited significantly higher tumor accumulation compared to RC.

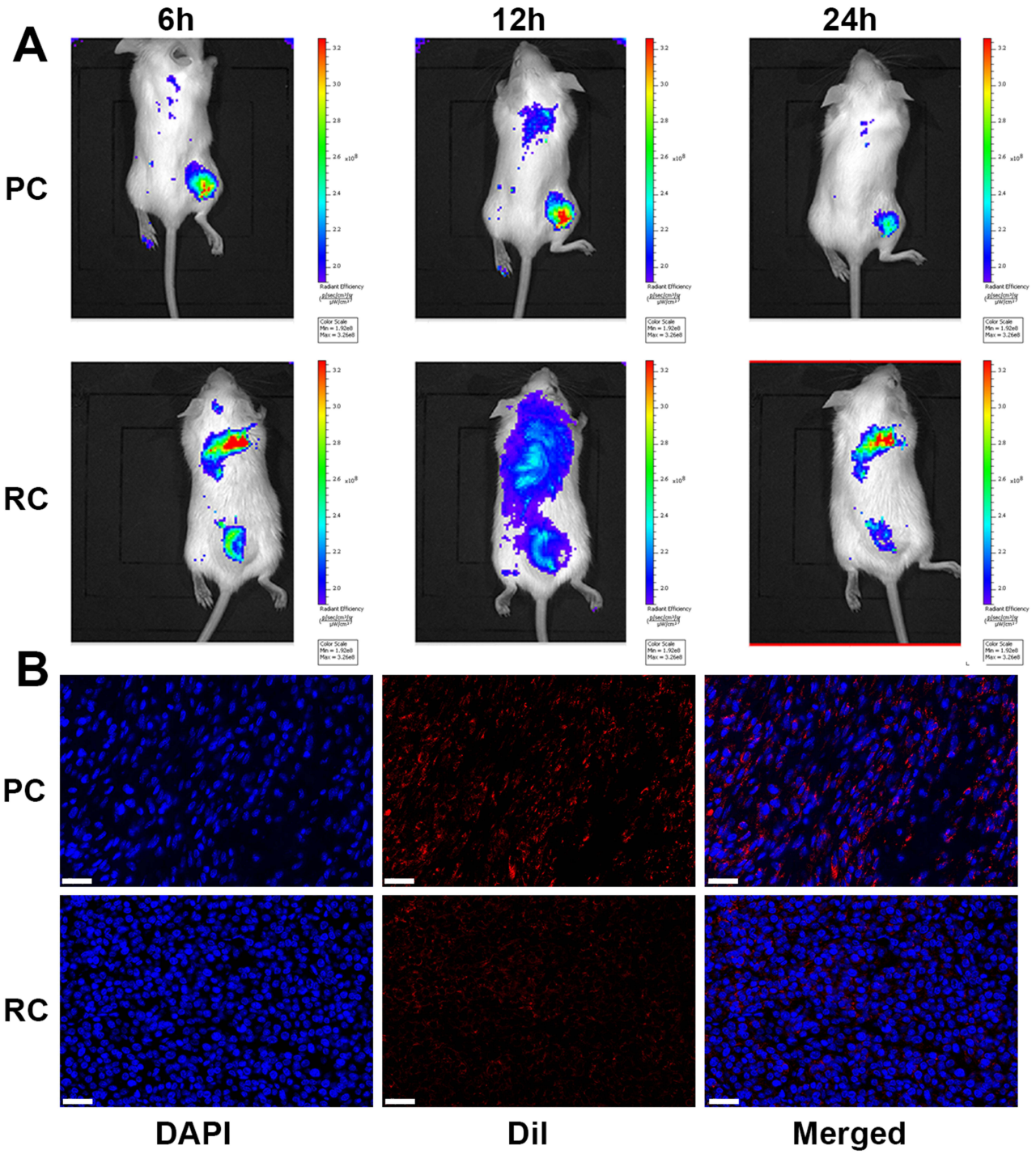

Figure 3 Tumor-specific targeting of PC. (**A**) Fluorescence imaging of mice administrated with PC or RC at different time intervals. (**B**) Immunofluorescence staining of tumors from mice treated with PC or RC (Scale bar: 30 μm).

Considering the favorable outcomes obtained from the aforementioned findings, the assessment of anti-tumor efficacy was conducted using a mouse model with subcutaneous tumors. After the tumor volume reached approximately 200 mm^3, mice were divided randomly into 5 groups and subjected to different treatments. As shown in Figure 4A, the result demonstrated rapid tumor growth in the control group. However, following

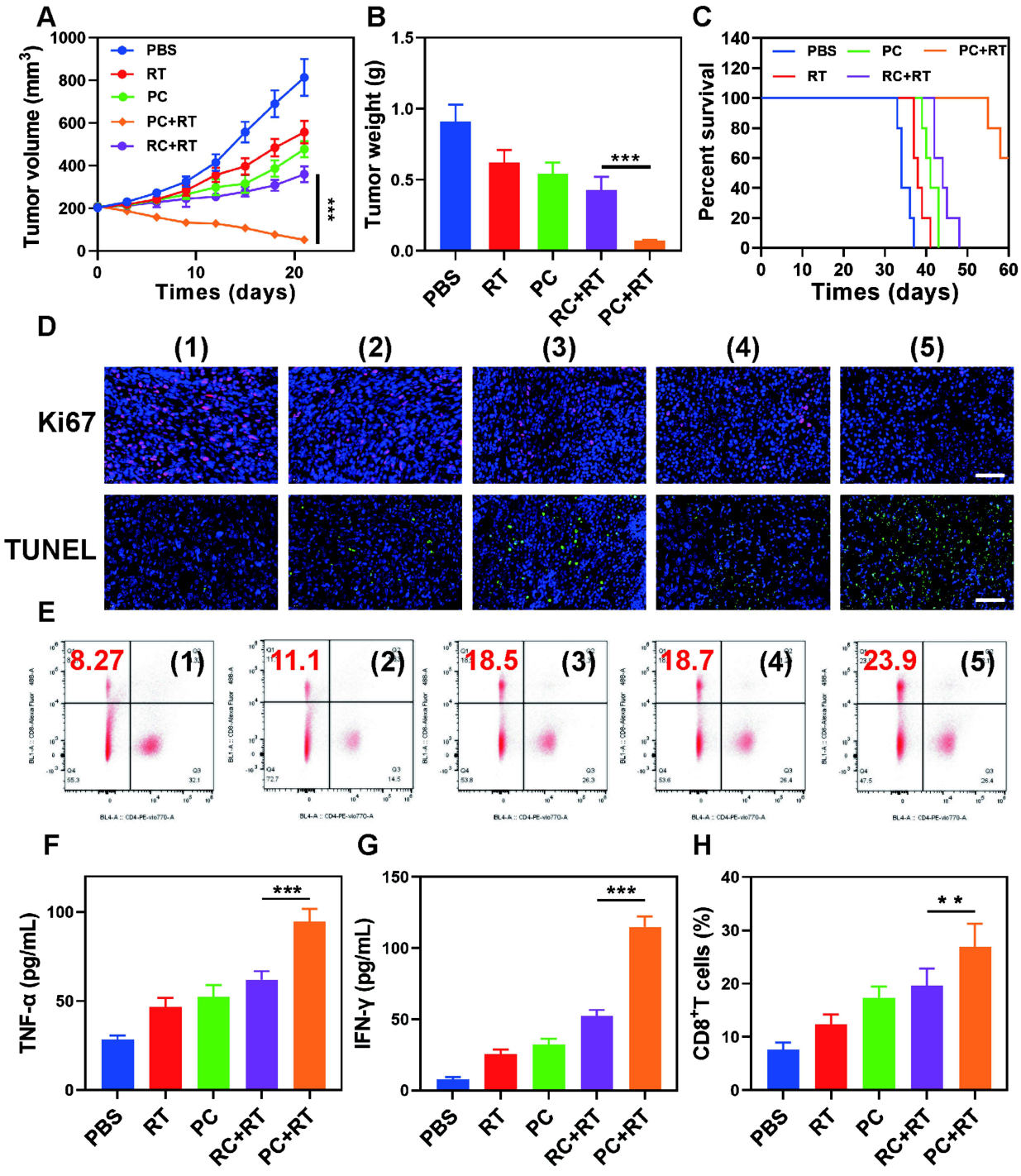

Figure 4 Antitumor efficacy through PC-mediated radioimmunotherapy. (**A**) Tumor volume, (**B**) tumor weight, and (**C**) survival curves in different treatment groups. (**D**) Ki 67 and Tunel staining of tumor tissues in different treatment groups ((1) PBS; (2) RT;(3) PC; (4) RC+RT; (5) PC+RT. Scale bar: 50 μm). (**E**) Flow cytometric analyses of the populations of $CD8^+$ and $CD4^+$ T cells in splenocytes of mice((1) PBS; (2) RT;(3) PC; (4) RC+RT; (5) PC+RT). Cytokine levels of (**F**) TNF-α and (**G**) IFN-γ in different groups evaluated by ELISA. (**H**) Populations of $CD8^+$ after different treatments. One-way ANOVA for multiple groups were applied for statistical analysis. ***p < 0.001.

treatment with either RT or PC alone, partial inhibition of tumor growth was observed. In the case of treatment with RC+RT, the tumor growth inhibition (TGI) reached 55.8%, signifying a relatively notable antitumor effect. However, in the group of mice treated with PC+RT, remarkable suppression of tumor growth was observed, with the TGI increasing to 93.6%. This outcome was consistent with the results related to tumor weight in Figure 4B. A long-term observation of the survival status of mice in each group was conducted (Figure 4C). A significantly prolonged survival time was observed in the PC+RT group, with a 60% survival rate at 60 days post-treatment. Representative ex vivo immunofluorescence images of tumors further confirmed the tumor cell proliferation (Ki-67) and tumor cell apoptosis (TUNEL) in each group (Figure 4D). The expression of Ki-67 was down-regulated, and TUNEL-positive cells were widely expressed in the PC+RT group. In additional, apparent damaged tumor tissue was observed in the PC+RT group as demonstrated in Figure S8. This suggests the feasibility of PC+RT in suppressing tumor growth.

Subsequently, we assessed the feasibility of PC-enhanced radiotherapy in activating immune therapy by examining the profiles of tumor-infiltrating lymphocytes in each treatment group. T cells were collected from tumor tissues and analyzed using flow cytometry. A notable increase in the content of $CD8^+$ and CD 4^+ was observed in the PC+RT group, as shown in Figure 4E, indicating an enhancement of cancer immunotherapy. Moreover, the quantification of cytokines involved in ICD, including tumor necrosis factors (TNF-α) in Figure 4F and interferon-γ (IFN-γ) in 4G, demonstrated an increase. This indicates that an immune response was indeed triggered. Furthermore, the PC+RT groups exhibited a significant release of an abundant amount of $CD8^+$ T cells through the activation of the immune response, in comparison to the other treatment groups (Figure 4H). This could be attributed to the immune evasion and cancer-targeting capabilities of these nanoparticles.

Ensuring the biosafety of PC is crucial prior to clinical use. In this regard, healthy mice were administered with either PBS or PC NPs via the tail vein. Thirty days after the injection, blood samples were collected from the orbital venous plexus of each mouse. Subsequently, the mice were euthanized, and their organs were harvested. Representative images of hematoxylin and eosin (HE) staining in the two groups are presented in Figure 5A. It is evident from the images that no significant injuries or lesions were observed in the main organs of both groups,

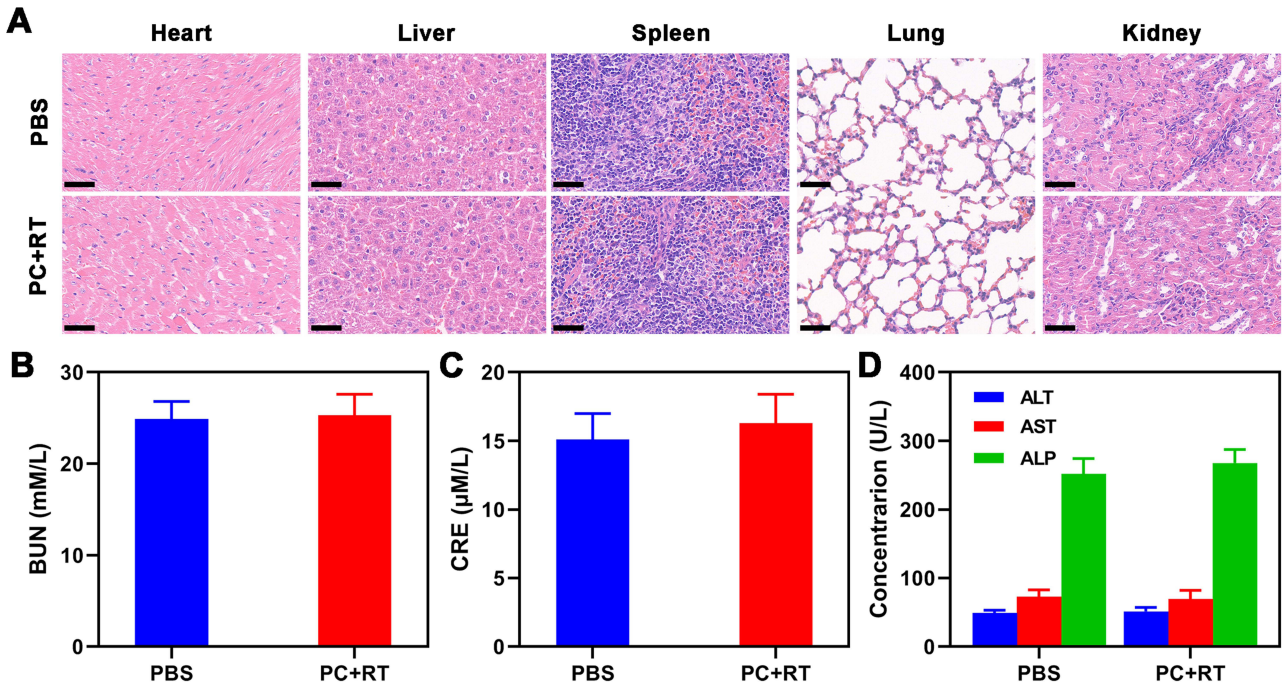

Figure 5 Biosafety evaluation. (**A**) Representative HE staining images of the main organs (Scale bar: 50 μm). (**B**) Blood urea nitrogen (BUN), (**C**) creatinine (CRE), and (**D**) alanine aminotransferase (ALT), aspartate aminotransferase (AST), and alkaline phosphatase (ALP).

indicating that PC did not cause any damage to these organs. Additionally, a blood routine analysis was conducted on these blood samples, and the results are displayed in Figure 5B–D. No significant differences were observed in the blood routine data, including blood urea nitrogen (BUN), creatinine (CRE), alanine aminotransferase (ALT), aspartate aminotransferase (AST), and alkaline phosphatase (ALP), between the two groups. These results confirm the biocompatibility of PC.

Conclusion

In summary, we developed a platelet cell membrane-camouflaged Cu SAzyme, termed PC, to enhance the radiosensitization of breast tumors. PC has demonstrated excellent biocompatibility both in vitro and in vivo. Compared to RC, which is coated with the red blood cell membrane, PC can actively target tumor regions, due to the surface modification with the platelet cell membrane. Tumor cells often develop resistance to radiotherapy because the ROS generated through ionization can be neutralized by the reducing tumor microenvironment, ultimately resulting in the failure of radiotherapy. With its POD-mimicking properties, PC generates an abundant supply of ROS from the intracellularly overexpressed H_2O_2 in tumor cells, thereby complementing the levels of ROS for effective tumor therapy. It is surprising to discover that PC-enhanced radiotherapy activates an immune response by enhancing the population of $CD8^+$ T cells and increasing the levels of cytokines TNF-α and IFN-γ. The results from both in vitro and in vivo experiments demonstrate remarkable tumor suppression. Therefore, this platelet-mimicking nanozyme provides novel strategy to enhance radioimmunotherapy for breast cancer treatment. Multiple animal models should be tested to further verify the therapeutic efficacy before clinical application.

Acknowledgments

Cheng Chen, Nandi Chen, Yan Qi and Chaoyan Wu contributed equally to this work. The authors would like to thank all the reviewers who participated in the review and MJEditor (www.mjeditor.com) for its linguistic assistance during the preparation of this manuscript.

Funding

This work was financially supported by National Natural Science Foundation of China (Grant No. 82073349), the Technology & Innovation Commission of Shenzhen Municipality (Shenzhen, China, Grant No. JCYJ20190807145011340), and Shenzhen High-tech Development Special Plan-Pingshan District Innovation Platform Project (29853M-KCJ-2023-002-04).

Disclosure

The authors report no conflicts of interest in this work.

References

1. Giaquinto AN, Sung H, Miller KD, et al. Breast cancer statistics, 2022. *Ca a Cancer J Clinicians*. 2022;72(6):524–541. doi:10.3322/caac.21754
2. Katsura C, Ogunmwonyi I, Kankam HKN, Saha S. Breast cancer: presentation, investigation and management. *Br J Hosp Med*. 2022;83(2):1–7. doi:10.12968/hmed.2021.0459
3. Kunkler IH, Williams LJ, Jack WJL, Cameron DA, Dixon JM. Breast-conserving surgery with or without irradiation in early breast cancer. *N Engl J Med*. 2023;388(7):585–594. doi:10.1056/NEJMoa2207586
4. Group EBCTC. Effect of radiotherapy after breast-conserving surgery on 10-year recurrence and 15-year breast cancer death: meta-analysis of individual patient data for 10,801 women in 17 randomised trials. *Lancet*. 2011;378(9804):1707–1716. doi:10.1016/S0140-6736(11)61629-2
5. Whelan TJ, Smith S, Parpia S, et al. Omitting radiotherapy after breast-conserving surgery in luminal a breast cancer. *N Engl J Med*. 2023;389(7):612–619. doi:10.1056/NEJMoa2302344
6. Yadav P, Shankar BS. Radio resistance in breast cancer cells is mediated through TGF-β signalling, hybrid epithelial-mesenchymal phenotype and cancer stem cells. *Biomed Pharmacother*. 2019;111:119–130. doi:10.1016/j.biopha.2018.12.055
7. Troschel FM, Palenta H, Borrmann K, et al. Knockdown of the prognostic cancer stem cell marker musashi-1 decreases radio-resistance while enhancing apoptosis in hormone receptor-positive breast cancer cells via p21WAF1/CIP1. *J Cancer Res Clin Oncol*. 2021;147(11):3299–3312. doi:10.1007/s00432-021-03743-y
8. Wang M, Chang M, Li C, et al. Tumor-microenvironment-activated reactive oxygen species amplifier for enzymatic cascade cancer starvation/chemodynamic/immunotherapy. *Adv Mater*. 2022;34(4):2106010. doi:10.1002/adma.202106010

9. Pan W-L, Tan Y, Meng W, et al. Microenvironment-driven sequential ferroptosis, photodynamic therapy, and chemotherapy for targeted breast cancer therapy by a cancer-cell-membrane-coated nanoscale metal-organic framework. *Biomaterials*. 2022;283:121449. doi:10.1016/j.biomaterials.2022.121449
10. Zhu Y, Wang W, Cheng J, et al. Stimuli-responsive manganese single-atom nanozyme for tumor therapy via integrated cascade reactions. *Angew Chem Int Ed*. 2021;60(17):9480–9488. doi:10.1002/anie.202017152
11. Siddique S, Chow JCL. Recent advances in functionalized nanoparticles in cancer theranostics. *Nanomaterials*. 2022;12(16):2826. doi:10.3390/nano12162826
12. Siddique S, Chow JCL. Application of nanomaterials in biomedical imaging and cancer therapy. *Nanomaterials*. 2020;10(9):1700. doi:10.3390/nano10091700
13. Wang Q, Liu J, He L, Liu S, Yang P. Nanozyme: a rising star for cancer therapy. *Nanoscale*. 2023;15(30):12455–12463. doi:10.1039/D3NR01976D
14. Li S, Shang L, Xu B, et al. A nanozyme with photo-enhanced dual enzyme-like activities for deep pancreatic cancer therapy. *Angew Chem Int Ed*. 2019;58(36):12624–12631. doi:10.1002/anie.201904751
15. Lyu M, Luo M, Li J, et al. Personalized carbon monoxide-loaded biomimetic single-atom nanozyme for ferroptosis-enhanced flash radioimmunotherapy. *Adv Funct Mater*. 2023;33(51):2306930. doi:10.1002/adfm.202306930
16. Wang Z, Li Z, Sun Z, et al. Visualization nanozyme based on tumor microenvironment "unlocking" for intensive combination therapy of breast cancer. *Sci Adv*. 2020;6(48):eabc8733. doi:10.1126/sciadv.abc8733
17. Gao L, Zhuang J, Nie L, et al. Intrinsic peroxidase-like activity of ferromagnetic nanoparticles. *Nat Nanotechnol*. 2007;2(9):577–583. doi:10.1038/nnano.2007.260
18. Wu C, Xu D, Ge M, et al. Blocking glutathione regeneration: inorganic NADPH oxidase nanozyme catalyst potentiates tumoral ferroptosis. *Nano Today*. 2022;46:101574. doi:10.1016/j.nantod.2022.101574
19. Wang P, Liu S, Hu M, et al. Peroxidase-like nanozymes induce a novel form of cell death and inhibit tumor growth in vivo. *Adv Funct Mater*. 2020;30(21):2000647. doi:10.1002/adfm.202000647
20. Zhang R, Xue B, Tao Y, et al. Edge-site engineering of defective fe–n4 nanozymes with boosted catalase-like performance for retinal vasculopathies. *Adv Mater*. 2022;34(39):2205324. doi:10.1002/adma.202205324
21. Zhang Y, Gao W, Ma Y, et al. Integrating pt nanoparticles with carbon nanodots to achieve robust cascade superoxide dismutase-catalase nanozyme for antioxidant therapy. *Nano Today*. 2023;49:101768. doi:10.1016/j.nantod.2023.101768
22. Li W, Song Y, Liang X, et al. Mutual-reinforcing sonodynamic therapy against rheumatoid arthritis based on sparfloxacin sonosensitizer doped concave-cubic rhodium nanozyme. *Biomaterials*. 2021;276:121063. doi:10.1016/j.biomaterials.2021.121063
23. Zhu D, Ling R, Chen H, et al. Biomimetic copper single-atom nanozyme system for self-enhanced nanocatalytic tumor therapy. *Nano Res*. 2022;15(8):7320–7328. doi:10.1007/s12274-022-4359-6
24. Zhu D, Chen H, Huang C, et al. H2O2 self-producing single-atom nanozyme hydrogels as light-controlled oxidative stress amplifier for enhanced synergistic therapy by transforming "cold" tumors. *Adv Funct Mater*. 2022;32(16):2110268. doi:10.1002/adfm.202110268
25. Liu Y, Wang B, Zhu J, Xu X, Zhou B, Yang Y. Single-atom nanozyme with asymmetric electron distribution for tumor catalytic therapy by disrupting tumor redox and energy metabolism homeostasis. *Adv Mater*. 2023;35(9):2208512. doi:10.1002/adma.202208512
26. Cai S, Liu J, Ding J, et al. Tumor-microenvironment-responsive cascade reactions by a cobalt-single-atom nanozyme for synergistic nanocatalytic chemotherapy. *Angew Chem Int Ed*. 2022;61(48):e202204502. doi:10.1002/anie.202204502
27. Liu J, Cabral H, Song B, et al. Nanoprobe-based magnetic resonance imaging of hypoxia predicts responses to radiotherapy, immunotherapy, and sensitizing treatments in Pancreatic Tumors. *ACS Nano*. 2021;15(8):13526–13538. doi:10.1021/acsnano.1c04263
28. Laprise-Pelletier M, Simão T, Fortin M-A. Gold nanoparticles in radiotherapy and recent progress in nanobrachytherapy. *Adv Healthcare Mater*. 2018;7(16):1701460. doi:10.1002/adhm.201701460
29. Feng L, Dong Z, Liang C, et al. Iridium nanocrystals encapsulated liposomes as near-infrared light controllable nanozymes for enhanced cancer radiotherapy. *Biomaterials*. 2018;181:81–91. doi:10.1016/j.biomaterials.2018.07.049
30. Haume K, Rosa S, Grellet S, et al. Gold nanoparticles for cancer radiotherapy: a review. *Cancer Nanotechnol*. 2016;7(1):8. doi:10.1186/s12645-016-0021-x
31. Azharuddin M, Zhu GH, Das D, et al. A repertoire of biomedical applications of noble metal nanoparticles. *Chem Commun*. 2019;55(49):6964–6996. doi:10.1039/c9cc01741k
32. Zhu Y, Jin D, Liu M, et al. Oxygen self-supply engineering-ferritin for the relief of hypoxia in tumors and the enhancement of photodynamic therapy efficacy. *Small*. 2022;18(15):2200116. doi:10.1002/smll.202200116
33. Lu N, Fan W, Yi X, et al. Biodegradable hollow mesoporous organosilica nanotheranostics for mild hyperthermia-induced bubble-enhanced oxygen-sensitized radiotherapy. *ACS Nano*. 2018;12(2):1580–1591. doi:10.1021/acsnano.7b08103
34. Wang M, Chang M, Zheng P, et al. A noble auptag-gox nanozyme for synergistic tumor immunotherapy induced by starvation therapy-augmented mild photothermal therapy. *Adv Sci*. 2022;9(31):2202332. doi:10.1002/advs.202202332
35. Yao L, Zhao -M-M, Luo Q-W, et al. carbon quantum dots-based nanozyme from coffee induces cancer cell ferroptosis to activate antitumor immunity. *ACS Nano*. 2022;16(6):9228–9239. doi:10.1021/acsnano.2c01619
36. Lyu M, Chen M, Liu L, et al. A platelet-mimicking theranostic platform for cancer interstitial brachytherapy. *Theranostics*. 2021;11(15):7589–7599. doi:10.7150/thno.61259
37. Lyu M, Zhang T, Li Y, et al. AIEgen-based nanotherapeutic strategy for enhanced FLASH irradiation to prevent tumour recurrence and avoid severe side effects. *Chem Eng J*. 2023;473:145179. doi:10.1016/j.cej.2023.145179
38. Dehaini D, Wei X, Fang RH, et al. Erythrocyte–platelet hybrid membrane coating for enhanced nanoparticle functionalization. *Adv Mater*. 2017;29(16):1606209. doi:10.1002/adma.201606209
39. Hara Y, Steiner M, Baldini MG. Characterization of the platelet-aggregating activity of tumor cells. *Cancer Res*. 1980;40(4):1217–1222.